Iterative Learning Control for Vibration Reduction in Industrial Robots with Link Flexibility

Chi-Shen Tsai[1], Wenjie Chen[1], Daekyu Yun[2], and Masayoshi Tomizuka[1]

Abstract— **This paper proposes an iterative learning control (ILC) scheme for the reduction of the end-effector vibration caused by the flexible link deflection in large-size robot manipulators. A 6-DoF LCD substrate transfer robot with two long vertical links is used as the testing example to study the end-effector vibration reduction. Due to the beam flexibility of the long vertical links, the precision performance of the end-effector may be severely degraded especially when robots are out-stretching. Normally there is no actuation degree of freedom on the link of deflection to directly compensate for the vibration. Hence, control action is applied to other actuation degrees of freedom based on the kinematic study of the vibration. Specifically, an ILC scheme is employed to off-line modify the reference trajectory of these robot joints for the next iteration based on prior position measurements of the end-effector and the kinematic relationships between the joints and the end-effector. Simulation results demonstrate the superior performance of the proposed scheme in reducing the vibration of the end-effector.**

I. Introduction

Robot manipulators have been broadly utilized in industry to convey parts in assembly lines. In some assembly lines, work-pieces being conveyed are large and fragile and thus the sizes of robot manipulators for handling these conveying tasks are large as well. The LCD manufacturing is such an example. LCD substrates are glasses of the size of, take 7.5G for instance, 1.95 m and 2.25 m in width and length but only 2 mm in thickness [1]. Hence LCD substrates are very fragile and require careful attention on handling. Robots for conveying LCD substrates between the assembly line and the storage cassette for later transport or storage play important roles in the manufacturing process. During the transport process, any fracture of LCD substrates lowers the production quality of the manufacturing process and thus is highly undesirable. On the other hand, the LCD substrate transfer robots are desired to convey LCD substrates at a higher transferring speed to increase the manufacturing productivity while maintaining a high precision quality. Moreover, the LCD substrate transfer robots are increased in size for new generation to accommodate for the growing size of LCD substrates. As the size of robots becomes larger, transmission mechanisms at the robot joints may pronounce the joint elasticity. Also, the flexibility of large robot links can no longer be neglected. These issues will induce vibration at the end-effector during the motion of robots. The bottleneck of conveying process occurs at the stage of loading/unloading LCD substrates because the width of the storage cassette is normally about 30 mm larger than the width of the LCD substrate.

The above issues indicate that the flexibility study and the vibration control for robots with these flexibilities are desired. [2] proposed a dynamic model for joint flexibility of the robot with three serial arms driven by one motor via two timing belts. This type of robot [3] is largely employed in the LCD manufacturing industry. For link flexibility, the finite-element analysis (FEA) method can be used to model the flexible links and obtain their frequency responses [4]. A simpler method when FEA method is not available is the lumped-parameter method [4] which approximates a flexible body as a set of rigid bodies coupled with springs and dampers. For control purpose, however, these dynamic models are generally too complex to be utilized for computationally efficient control. Therefore, other control strategies need to be utilized.

In existing literature, a well-known control method to handle residual vibrations is input shaping [5]. It reduces the vibration by feedforward compensation for the dominant system modes. However, this method may lose its applicability when the dominant vibration modes are subject to change due to the time-varying system dynamics in a typical out-stretching trajectory. Thus, it is desired that the controller should be able to continuously learn the vibration behavior for trajectories of time-varying vibration characteristics. Moreover, industrial robots are often designed for performing the same task repeatedly. In such cases, learning controllers can utilize the repetitive nature to improve performance. Iterative learning control (ILC) is such a feedforward control strategy which aims to compensate for repetitive errors in the task based on the error information learned from previous cycles and to enhance the performance of the motion for the next cycle [6], [7]. Various ILC schemes have been studied and widely applied to many practical problems. In this paper, a serial ILC scheme which adjusts the reference trajectories for the next iteration is utilized. By doing this, we can avoid direct access to the control input of the robot and hence the off-line ILC controller can be separated from the original robot real-time feedback controller.

The outline of this paper is as follows. In Section II, the dynamic model of the multi-joint robot with joint elasticity is introduced. Then a LCD substrate transfer robot is used as an example and the kinematic study of the vibration induced by robot link flexibility is investigated. In Section III, a

This work was supported by Hyundai Heavy Industries Co., LTD, Korea.

[1]Chi-Shen Tsai, Wenjie Chen, and Masayoshi Tomizuka are with the Department of Mechanical Engineering, University of California, Berkeley, CA 94720, USA. {cstsai, wjchen, tomizuka}@me.berkeley.edu

[2] Daekyu Yun is with Hyundai Heavy Industries Co., LTD, Korea. {eorbking@naver.com}

serial ILC scheme with the learning filter design is presented. The vibration compensation based on the kinematic study is shown next. Subsequently, the simulation results are presented in Section IV to validate the proposed scheme. The conclusion is given in Section V at last.

II. Robot Dynamic Model

A. Dynamic Model of an Elastic Joint

In practice, for the purpose of torque amplification, large-size robots normally use an indirect drive train with one or more levels of transmission mechanisms in each joint. Fig. 1 shows the schematic of the indirect drive train model for an elastic joint with two levels of transmission mechanisms. The dynamic model of this joint can be formulated as

$$J_m\ddot{\theta}_m + d_m\dot{\theta}_m = u - f_{mc}\text{sgn}(\dot{\theta}_m) - \frac{1}{N_1}\left[k_{r1}\left(\frac{\theta_m}{N_1} - \theta_i\right) + d_{r1}\left(\frac{\dot{\theta}_m}{N_1} - \dot{\theta}_i\right)\right] \quad (1)$$

$$J_i\ddot{\theta}_i + d_i\dot{\theta}_i = \left[k_{r1}\left(\frac{\theta_m}{N_1} - \theta_i\right) + d_{r1}\left(\frac{\dot{\theta}_m}{N_1} - \dot{\theta}_i\right)\right] - \frac{1}{N_2}\left[k_{r2}\left(\frac{\theta_i}{N_2} - \theta_l\right) + d_{r2}\left(\frac{\dot{\theta}_i}{N_2} - \dot{\theta}_l\right)\right] - f_{ic}\text{sgn}(\dot{\theta}_i) \quad (2)$$

$$J_l\ddot{\theta}_l + d_l\dot{\theta}_l = \left[k_{r2}\left(\frac{\theta_i}{N_2} - \theta_l\right) + d_{r2}\left(\frac{\dot{\theta}_i}{N_2} - \dot{\theta}_l\right)\right] - f_{lc}\text{sgn}(\dot{\theta}_l) - \tau_r \quad (3)$$

where all the parameters are defined in Fig. 1. In the practical controller design and analysis, however, a simplified model with only one transmission mechanism, which is sufficient to capture major dynamic characteristics, is usually preferred in order to reduce the design and computation complexity. To do this, the intermediate component and the motor in Fig. 1 are combined into an equivalent motor, and the two transmission mechanisms are replaced by one equivalent transmission mechanism. For this equivalent model structure, the equivalent gear ratio is the product of two gear ratios as $N_{eq} = N_1N_2$. The equivalent motor inertia J_{eq} can be obtained as $J_{eq} = J_m + \frac{1}{N_1^2}J_i$ by assuming the rigid connection of the first transmission mechanism. Similarly, the equivalent motor damping coefficient is obtained as $d_{eq} = d_m + \frac{1}{N_1^2}d_i$. Then the stiffness and the damping coefficients of the equivalent transmission mechanism can be computed with the assumption that the torques transmitted through two transmission mechanisms should be the same. By some algebraic manipulations, the equivalent stiffness and damping coefficients are obtained as

$$k_{req} = \left(\frac{1}{k_{r1}}\frac{1}{N_2^2} + \frac{1}{k_{r2}}\right)^{-1}, d_{req} = \left(\frac{1}{d_{r1}}\frac{1}{N_2^2} + \frac{1}{d_{r2}}\right)^{-1} \quad (4)$$

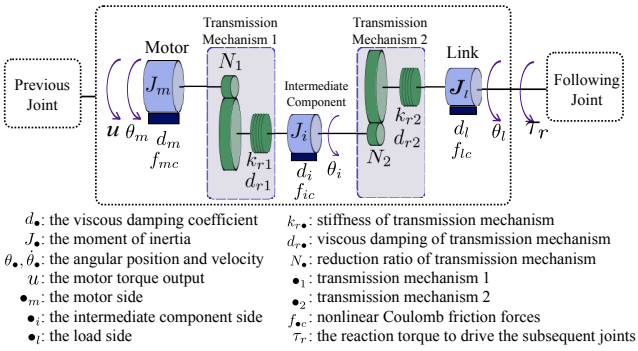

Fig. 1. An elastic joint with two levels of transmission mechanisms.

Therefore, the equivalent dynamic model is formulated as

$$J_{eq}\ddot{\theta}_m + d_{eq}\dot{\theta}_m = u - f_{mc}\text{sgn}(\dot{\theta}_m) - \frac{1}{N_{eq}}\left[k_{req}\left(\frac{\theta_m}{N_{eq}} - \theta_l\right) + d_{req}\left(\frac{\dot{\theta}_m}{N_{eq}} - \dot{\theta}_l\right)\right] \quad (5)$$

$$J_l\ddot{\theta}_l + d_l\dot{\theta}_l = \left[k_{req}\left(\frac{\theta_m}{N_{eq}} - \theta_l\right) + d_{req}\left(\frac{\dot{\theta}_m}{N_{eq}} - \dot{\theta}_l\right)\right] - f_{lc}\text{sgn}(\dot{\theta}_l) - \tau_r \quad (6)$$

Equations (5) and (6) provide a general dynamic model formulation for one robotic joint with transmission mechanisms. This model can be analogously extended to the multi-joint robot case. The inertia, Coriolis, and gravity terms of multi-joint robots, however, would need to be further synthesized from the Lagrangian dynamics study, as given in the next section.

B. Dynamic Model of Multi-joint Robot

From the model formulation (5) - (6) and the Lagrangian dynamics study, the dynamic model of an n-joint robot with gear compliance can be formulated as

$$M_l(q_l)\ddot{q}_l + C(q_l,\dot{q}_l)\dot{q}_l + G(q_l) + J^T(q_l)f_{ext} + F_{lc}\text{sgn}(\dot{q}_l) + D_l\dot{q}_l = K_J(N^{-1}q_m - q_l) + D_J(N^{-1}\dot{q}_m - \dot{q}_l) \quad (7)$$

$$M_m\ddot{q}_m + D_m\dot{q}_m + F_{mc}\text{sgn}(\dot{q}_m) = \tau_m - N^{-1}\left[K_J\left(N^{-1}q_m - q_l\right) + D_J\left(N^{-1}\dot{q}_m - \dot{q}_l\right)\right] \quad (8)$$

where q_l and q_m are the load side and the motor side position vectors, respectively. τ_m is the motor torque. $M_l(q_l)$ is the load side inertia matrix, $C(q_l,\dot{q}_l)$ is the Coriolis and centrifugal matrix, and $G(q_l)$ is the gravity vector. M_m, K_J, D_J, D_l, D_m, F_{lc}, F_{mc}, and N are all diagonal matrices, and the i-th diagonal term in each matrix represents the motor side inertia, joint stiffness, joint damping, load side damping, motor side damping, load side Coulomb friction, motor side Coulomb friction, and gear ratio of the i-th joint, respectively. f_{ext} denotes the external force acting on the robot end-effector due to the contact with the environment. The matrix $J(q_l)$ is the Jacobian matrix mapping from the load side joint space to the end-effector Cartesian space.

Note that all the matrices in the motor side dynamic model (8) are diagonal, while the inertia, Coriolis, gravity, and the Jacobian matrices at the load side model (7) are highly coupled amongst joints depending on the robot configuration. In order to implement a decentralized joint space control, we follow the decoupling procedure proposed in [8] to reformulate the robot dynamic model as an MIMO system with $2n$ inputs and $2n$ outputs described as

$$q_m(k) = P_{mu}(z)\tau_m(k) + P_{md}(z)d(k) \quad (9)$$

$$q_l(k) = P_{lu}(z)\tau_m(k) + P_{ld}(z)d(k) \quad (10)$$

where k is the time index, and z is the one time step advance operator in the discrete time. All coupling and nonlinear terms, such as Coriolis force, gravity, Coulomb frictions, and external forces, are grouped into a fictitious disturbance torque d. $P_{mu}(z)$, $P_{md}(z)$, $P_{lu}(z)$, and $P_{ld}(z)$ denote the transfer functions from the corresponding input (τ_m or d) to the corresponding output (q_m or q_l) respectively.

C. Kinematic Study of the End-effector Vibration

In the previous section, the robot dynamic model is built based on the assumption that the link deflection (including bending and twisting) is small enough to be negligible. This assumption, however, may not be valid for large-size robots, where the link deflection occurring in the motion results in vibrations especially on the end-effector. Thus, it is necessary to investigate the kinematics of the vibration caused by the link flexibility and take it into consideration in the control algorithm design. Link flexibility greatly depends on the mechanical design of the robot manipulator. A typical LCD substrate transfer robot shown in Fig. 2 is used here as an illustrating example.

This robot has 6 motors and 10 links distributed on 6 joints. In particular, Joint 5 is composed of a motor mounted on Link 4, and three horizontal links, Link 5, Link 6, and Link 7, which are connected in the serial order. With proper kinematic design and choice of reduction ratio, the end-effector, Link 7, moves on a straight line along the Y-axis. Similarly, Joint 6, composed of a motor, Link 8, Link 9, and Link 10, is designed to have the identical mechanical structure as that of Joint 5 for the purpose of handling two LCD substrate transport tasks at the same time. Joint 3 and Joint 4 are prismatic for Link 3 and Link 4 to move vertically along the Z-axis so that Joint 5 and Joint 6 can reach different heights. Link 2 rotates along the axis of Joint 2 parallel to the Z-axis and Joint 1 is for translation along the X-axis.

The two vertical links, Link 2 and Link 3, are normally considerably long, and the beam deflection effect is non-negligible. Thus during the motion of loading/unloading task of Joint 5 (or Joint 6), the counter torque from Link 5 (or Link 8) may twist Link 2 and Link 3 and consequently result in the vibration of the end-effector. From the experimental data of an actual robot, it is found that this vibration magnitude becomes larger when the loading/unloading task is executed at a higher height.

Fig. 3 shows the top-view of the robot when Joint 5 is executing the loading/unloading task. In the figure, the

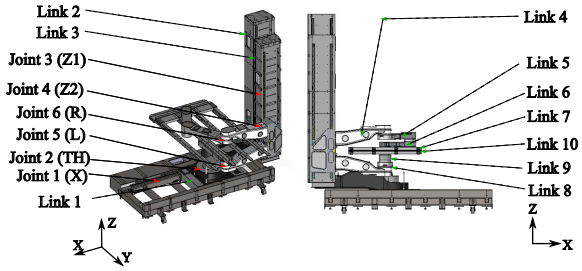

Fig. 2. The LCD substrate transfer robot structure.

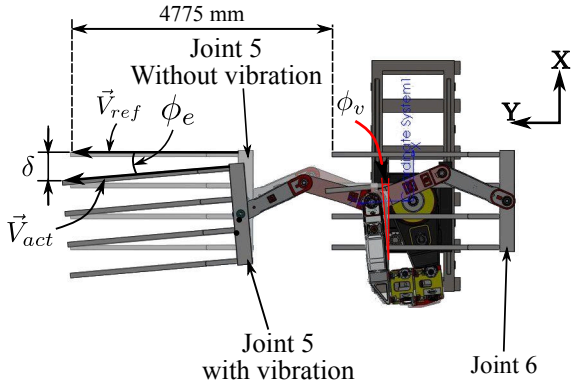

Fig. 3. Top-view of the LCD substrate transfer robot when the vertical links are twisted.

end-effector of Joint 5 in dark grey color represents an exaggerated position when the vertical links are twisted, while the one in light grey color shows the reference position when the vertical links are not twisted. Let δ be the position error along the X-axis of the tip point on the end-effector, ϕ_e be the angle error of the end-effector, and ϕ_v be the angle error of Link 4. Generally the vibration caused by the stiffness and the damping of the transmission mechanisms in Joint 5 (or Joint 6) is relatively small since the gear reducers and sets of belt-pulley mechanisms used in these joints are often with very high stiffness and damping. Hence ϕ_e is very close to ϕ_v.

Consider that there are two position sensors (e.g., laser optical tracker) for measuring the tip and the base point positions on the end-effector. This kind of sensing is normally available in addition to motor encoder sensing during the robot manufacturing and tuning stages. Therefore, the angle error of the end-effector, ϕ_e, can be derived by utilizing the position measurements of the two points on the end-effector. In Fig. 3, $\vec{V}_{act}$ is the vector from the actual base point position to the actual tip point position on the end-effector and $\vec{V}_{ref}$ is computed in the same way using the reference positions of the end-effector. Then ϕ_e can be computed as

$$\phi_e = \arccos \frac{\vec{V}_{act} \cdot \vec{V}_{ref}}{|\vec{V}_{act}|\,|\vec{V}_{ref}|} \quad (11)$$

Fig. 4 (a) shows the simulation results (see Section IV for the details of simulation model developement) of the position errors of the tip and the base points along the X-axis

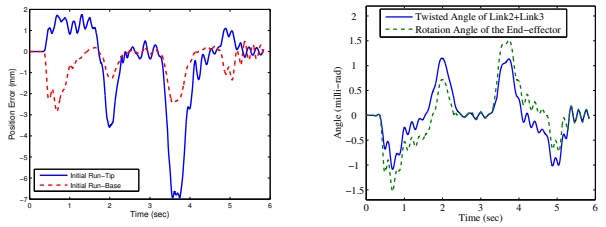

(a) (b)

Fig. 4. Comparison between the twisting angle of the vertical links and the rotation angle of the end-effector of Joint 6 in loading/unloading task in simulation.

when Joint 6 is executing the loading/unloading task. The corresponding angle error of the end-effector, ϕ_e, computed using (11) is shown as the dashed line in Fig. 4 (b). The sum of the twisting angles of Link 2 and Link 3 is also obtained from the simulation and plotted as the solid line in Fig. 4 (b). It shows that these two lines share a very similar pattern and are only slightly different in the peak values. This slight difference may be caused by the elasticity of the transmission mechanisms in Joint 6. Same observation and conclusion can be made for Joint 5. This confirms again that ϕ_e is very close to ϕ_v. Note that ϕ_e in (11) is derived based on the assumption that two position sensors are available on the end-effector. However, ϕ_e can still be computed with only one position sensor by assuming that the rotation center of the end-effector is invariant during a short period of time. In this case, the rotation center for that short time period can be computed by triangulation using the position measurements. The overall rotation center can be approximated off-line by averaging the rotation centers of all short time periods along this trajectory.

III. ILC for End-Effector Vibration Reduction

A. ILC with Reference Update

To eliminate the vibration resulting from the link flexibility, a serial ILC scheme is applied. The block diagram of the serial ILC scheme is shown in Fig. 5, and the ILC law can be expressed as

$$r_{j+1}^{ILC}(k) = Q_{ILC}(z)\left[r_j^{ILC}(k) + L(z)e_j(k)\right] \tag{12}$$

where j denotes the iteration index. The serial ILC scheme alters the reference trajectory rather than the control input to the robot plant as follows

$$r_{j+1}(k) = r(k) + r_{j+1}^{ILC}(k) \tag{13}$$

where $r(k)$ is the original reference trajectory. The benefit of the serial ILC scheme is to avoid direct access to the control input to the plant and hence the ILC controller can be separated from the original robot real-time feedback controller.

B. Compensation of the Vibration in the End-Effector

The position errors for each iteration, $e_j(k)$ in (12), are to be learned and reduced by ILC. However, if the joint where

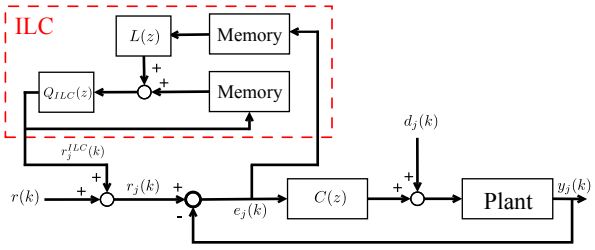

Fig. 5. The serial iterative learning control scheme. [6]

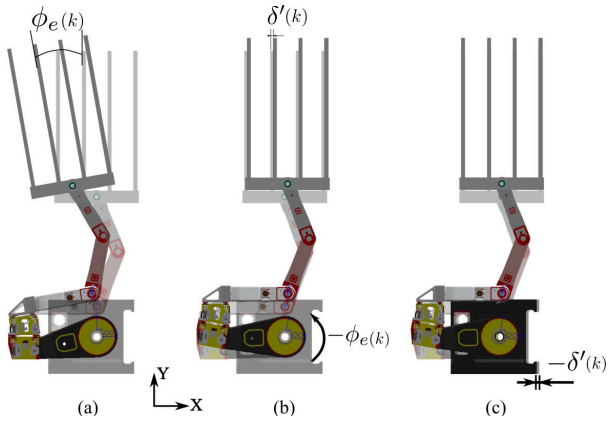

Fig. 6. Vibration reduction by modifying positions of Joint 1 and Joint 2.

the error exhibits does not have available actuation to directly compensate for this error, the actuation degrees of freedom of other joints may be utilized for active compensation.

In the aforementioned LCD substrate transfer robot, during the motion of loading/unloading task, the vibration of the end-effector in the X-Y plane is resulted from the twists of Link 2 and Link 3 caused by the counter torque of motors at Joint 5 and Joint 6. Since there are no rotational actuation in these vertical links (i.e., Link 2 and Link 3) to directly compensate for these rotational vibrations, the actuations of both Joint 1 and Joint 2 are utilized instead to actively compensate for the end-effector vibration, i.e., the serial ILC scheme is utilized to alter the reference trajectories of these two joints.

Fig. 6 (a) shows the reference position (in light grey color) and the actual position (in dark grey color) with an exaggerated end-effector vibration at the k-th time step with the angle error of the end-effector denoted as $\phi_e(k)$. This angle error can be corrected by rotating Joint 2 by $-\phi_e(k)$, as shown in Fig. 6 (b). Recall that $\phi_e(k)$ can be computed by (11). After this angle correction, the end-effector shown in dark grey color in Fig. 6 (b) is parallel to the reference position (in light grey color). The remaining offset error, $\delta'(k)$, between the new position and the reference position shown in Fig. 6 (b), can be computed as

$$\delta'(k) = \left(P_{tc}(k) - P_{tr}(k)\right) \cdot \vec{i} \tag{14}$$

where $P_{tc}(k)$ is the tip point position in the X-Y plane after compensation by rotation of $-\phi_e(k)$ with respect to the axis

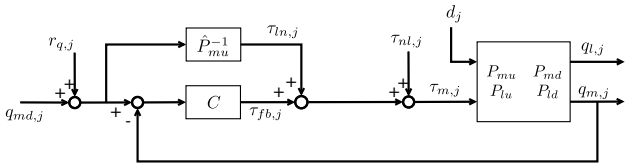

Fig. 7. The controller structure of the LCD substrate transfer robot.

of Joint 2. $P_{tr}(k)$ is the reference tip point position in the X-Y plane at the k-th time step. $\vec{i}$ is the unit vector along the X-axis. Thus, $P_{tc}(k)$ can be obtained as

$$P_{tc}(k) = O_{J2} + R(k)(P_{ta}(k) - O_{J2}) \tag{15}$$

where O_{J2} is the position of rotation axis of Joint 2 in the X-Y plane, $P_{ta}(k)$ is the actual tip position in the X-Y plane, and $R(k)$ is the rotation matrix defined as

$$R(k) = \begin{bmatrix} \cos(\phi_e(k)) & \sin(\phi_e(k)) \\ -\sin(\phi_e(k)) & \cos(\phi_e(k)) \end{bmatrix} \tag{16}$$

Then the actuation of Joint 1 can be utilized to correct the offset, $\delta'(k)$. Fig. 6 (c) shows the final position of the end-effector after the compensation through Joint 1 and Joint 2, where the position error along the X-axis is reduced.

The errors defined in (11) and (14) become the essential errors to be learned by the serial ILC scheme for Joint 1 and Joint 2 references. This leads to the following ILC scheme

$$r_{J1,j+1}^{ILC}(k) = Q_{J1}(z)\left[r_{J1,j}^{ILC}(k) + L_{J1}(z)(-\delta'(k))\right] \tag{17}$$
$$r_{J2,j+1}^{ILC}(k) = Q_{J2}(z)\left[r_{J2,j}^{ILC}(k) + L_{J2}(z)(-\phi_e(k))\right] \tag{18}$$

where the subscripts J1 and J2 denote Joint 1 and Joint 2. Note that Fig. 6 shows one typical posture for the loading/unloading task. There may be some other different postures for this kind of task. Similar ILC scheme with error computation can easily be derived for those postures.

C. The Structure of Overall Controller

Fig. 7 shows the controller structure of the robot manipulator system with the serial ILC scheme. The robot is reformulated as a MIMO system in (9) and (10). $\tau_{ln,j}$ and $\tau_{nl,j}$ are the linear and the nonlinear parts of the model based feedforward torque[1]. $\tau_{fb,j}$ is the feedback torque generated by a decoupled feedback controller C. $r_{q,j}$ is the additional reference trajectory generated by ILC for the j-th iteration. $q_{md,j}$ is the motor side reference trajectory for the j-th iteration, which is generated from the desired load side position reference, $q_{ld,j}$, as

$$q_{md,j} = \hat{P}_{mu}\hat{P}_{lu}^{-1} q_{ld,j} \tag{19}$$

where $\hat{\bullet}$ denotes the nominal model representation of $\bullet$. Note that the objective is to let $q_{l,j}$ track $q_{ld,j}$, even though the real-time feedback controller C is designed at the motor side for $q_{m,j}$ to track $q_{md,j}$.

[1]The feedforward torque $\tau_{ff,j} = \tau_{ln,j} + \tau_{nl,j}$ is computed by recursive Newton-Euler method for a given load side reference trajectory using Robotics Toolbox (RTB) [9] in MATLAB.

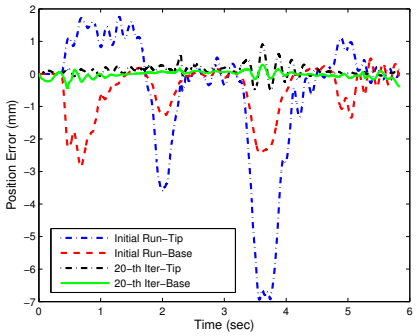

Fig. 8. Position error along the X-axis of the tip and the base points of Joint 6 for loading/unloading task in simulation.

D. The Learning Filter

From Fig. 7, $\tau_{m,j}$ can be obtained as

$$\tau_{m,j} = S_p\left[(q_{md,j}+r_{q,j})(\hat{P}_{mu}^{-1}+C)+\tau_{nl,j}-CP_{md}d_j\right] \tag{20}$$

where $S_p = (I + P_{mu}C)^{-1}$ is the sensitivity function of the closed loop system. By plugging $\tau_{m,j}$ into (9), q_l becomes

$$\begin{aligned} q_{l,j} =& P_{lu}S_p\left[(q_{md,j} + r_{q,j})(\hat{P}_{mu}^{-1} + C) + \tau_{nl,j} - CP_{md}d_j\right] \\ &+ P_{ld}d_j \end{aligned} \tag{21}$$

Manipulating (21) by substituting $\hat{P}_{mu}^{-1}\hat{S}_p^{-1}$ for $(\hat{P}_{mu}^{-1} + C)$ and noting (19), we obtain

$$\begin{aligned} q_{l,j} =& \hat{P}_{mu}^{-1}\, P_{lu}\, S_p\, \hat{S}_p^{-1}\, r_{q,j} + P_{ld}d_j + \\ & P_{lu}\, S_p\big(\hat{P}_{lu}^{-1}\, \hat{S}_p^{-1} q_{ld,j} + \tau_{nl,j} - CP_{md}d_j\big) \end{aligned} \tag{22}$$

Then the tracking error becomes

$$\begin{aligned} e_{l,j} =& q_{ld,j} - q_{l,j} \\ =& -\hat{P}_{mu}^{-1} P_{lu}\, S_p\, \hat{S}_p^{-1}\, r_{q,j} + \big(I_n - P_{lu}\, S_p\hat{P}_{lu}^{-1}\, \hat{S}_p^{-1}\big)q_{ld,j} \\ & - P_{lu}\, S_p\, \tau_{nl,j} + \big(P_{lu}S_pCP_{md} - P_{ld}\big)d_j \\ :=& -P_{eu}\, r_{q,j} + \bar{r}_{r,j} \end{aligned} \tag{23}$$

Therefore the tracking error can be improved by altering the reference trajectory iteratively with the optimal plant inverse learning filter as

$$L^*(z) = \hat{P}_{eu}^{-1}(z) = \hat{P}_{lu}^{-1}(z)\hat{P}_{mu}(z) \tag{24}$$

More details of the learning filter design and the stability of ILC scheme can be found in [8].

IV. Simulation Study

A dynamic simulator of the LCD substrate transfer robot is developed using MATLAB SimMechanics Toolbox based on the dynamic and the kinematic parameters as well as the CAD model of an actual Hyundai Heavy Industries LCD substrate transfer robot. For link flexibility simulation, Joint 3 is modeled as a cylindrical joint with two degrees of freedom (DoF) whose axes are parallel to the Z-axis. One DoF is the linear translation and the other is the rotation of the joint. The

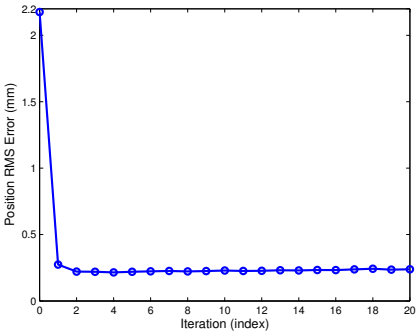

Fig. 9. RMS position error along the X-axis of the tip point in iteration domain.

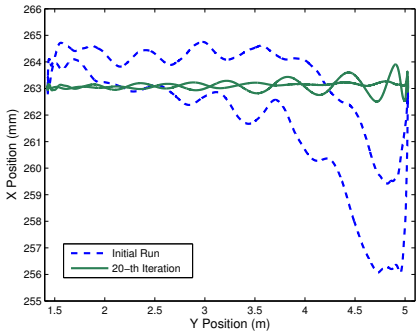

Fig. 10. Comparison of the motion of the tip point of Joint 6 in the X-Y plane between the initial run and the 20-th iterations.

torque output from the Joint 3 motor drives Link 3 and the subsequent joints to move along the axis of linear translation. The rotation of the cylindrical joint accounts for the twist of the link and is modeled by a torsional spring and a torsional damping. Joint 4 is modeled using the same method. The combination of Joint 3 and Joint 4 provides a large range of the operation height, from 1.6 m to 6.1 m. The experimental data from the actual robot shows the same pattern of the tracking error at the end-effector as shown in Fig. 4 (a). The developed robot dynamic model, (1) - (3), is utilized as the robot plant for simulation while the derived model, (9) and (10), is used for control purpose.

Simulations of the loading/unloading task executed by Joint 6 are conducted to validate the effectiveness of the proposed ILC scheme. It is noted that the frequency of major vibration is lower than 2 Hz. In order not to excite the high frequency elastic resonant mode, the Q-filter is chosen as a 5-th order zero phase low-pass filter with a cut-off frequency of 2 Hz. Fig. 8 shows the position errors along the X-axis of the tip and the base points on Joint 6 end-effector in the initial run and the 20-th iteration when the serial ILC scheme is applied.[2] The task is executed at the highest position for the robot hand. Compared to the position errors at the first iteration, which ranges from 2 to -7 mm, the error drastically decreases by 85.6%, to the level ranging from about 0.8 to -0.5 mm in the last iteration. The root-mean-square (RMS) position error along the X-axis of the tip point in each iteration is shown in Fig. 9. The RMS position error drops significantly from about 2 mm to about 0.3 mm in the first iteration and then gradually decreases to 0.2 mm. Thus the maximal vibration reduction is achieved in the first iteration and the error maintains stable convergence in the iteration domain. A comparison of the tip point motions in the X-Y plane between the initial run and the 20-th iteration is shown in Fig. 10, which demonstrates again the significant vibration reduction.

[2]20 iterations are plotted to show the stability of the serial ILC scheme, although the error reduction is achieved mainly within the first few iterations.

V. Conclusion

This paper proposed a serial ILC scheme for the end-effector performance enhancement for the large-size robots on which the links vibrate due to their flexible deflection. Normally there exist no actuation degrees of freedom to directly compensate for the vibration on these flexible links. Hence the control for vibration reduction was applied to the other joints by modifying the reference trajectories iteratively. In order to implement the learning scheme, the kinematic characteristic of the vibration was studied. The LCD substrate transfer robot was used as an example for the vibration kinematic study as well as the simulation validation. Based on the kinematic study of the LCD substrate transfer robot, the actuations of Joint 1 and Joint 2 were utilized in the ILC scheme to compensate for the vibration caused by the torsional deflection of the vertical links. The simulation results demonstrated that the developed ILC scheme can greatly reduce the end-effector vibration within the first few iterations.

References

[1] www.scp.samsung.com/product/prdLCD/prdHist.asp.
[2] R.-F. Fung, Y.-S. Kung, and G.-C. Wu, "Dynamic analysis and system identification of an LCD glass-handling robot driven by a pmsm," *Applied Mathematical Modelling*, vol. 34, no. 5, pp. 1360 – 1381, 2010.
[3] C. S. Lee, D. G. Lee, J. H. Oh, and H. S. Kim, "Composite wrist blocks for double arm type robots for handling large LCD glass panels," *Composite Structures*, vol. 57, no. 14, pp. 345 – 355, 2002.
[4] V. Chudnovsky, A. Mukherjee, J. Wendlandt, and D. Kennedy, "Modeling flexible bodies in simmechanics," Tech. Rep., August 2006.
[5] T. Singh and W. Singhose, "Input shaping/time delay control of maneuvering flexible structures," in *American Control Conference, 2002. Proceedings of the 2002*, vol. 3, 2002, pp. 1717 – 1731 vol.3.
[6] D. Bristow, M. Tharayil, and A. Alleyne, "A survey of iterative learning control," *Control Systems, IEEE*, vol. 6, no. 3, pp. 96 – 114, June 2006.
[7] R. Longman, "Iterative learning control and repetitive control for engineering practice," *International Journal of Control*, vol. 73, no. 10, pp. 930–954, 2000.
[8] W. Chen and M. Tomizuka, "Iterative learning control with sensor fusion for robots with mismatched dynamics and mismatched sensing," *Proceedings of the 2012 ASME Dynamic Systems and Control Conference (DSCC) and 2012 Motion & Vibration Conference (MOVIC)*, October 2012.
[9] P. Corke, "A robotics toolbox for matlab," *Robotics and Automation Magazine, IEEE*, vol. 3, no. 1, pp. 24–32, March 1996.